Chinese Chemical Letters 35 (2024) 108542

Contents lists available at ScienceDirect

Chinese Chemical Letters

journal homepage: www.elsevier.com/locate/cclet

# Molar ratio induced crystal transformation from coordination complex to coordination polymers

Peng Meng[a,1], Qian-Cheng Luo[b,1], Aidan Brock[a], Xiaodong Wang[c], Mahboobeh Shahbazi[a], Aaron Micallef[c], John McMurtrie[a], Dongchen Qi[a], Yan-Zhen Zheng[b,*], Jingsan Xu[a,*]

[a] School of Chemistry and Physics & Centre for Materials Science, Queensland University of Technology, Brisbane, QLD 4000, Australia
[b] Frontier Institute of Science and Technology, Xi'an Jiaotong University, Xi'an 710054, China
[c] Central Analytical Research Facility, Institute for Future Environments, Queensland University of Technology, Brisbane, QLD 4000, Australia

ARTICLE INFO

*Article history:*
Received 15 March 2023
Revised 23 April 2023
Accepted 5 May 2023
Available online 8 May 2023

*Keywords:*
Molar ratio dependent crystal transformation
Copper cyanurate
Ostwald ripening
Molecular magnetism
One-dimensional chain

ABSTRACT

Coordination complex of a copper cyanurate (Cu(II)-CA) was transformed into coordination polymers upon the stimulus of extra Cu(II) through "directed Ostwald ripening". By increasing the molar ratio of Cu(II) to CA, we obtained two coordination polymers with selective coordination sites: Cu(II)-$\kappa$N(HCA)$\kappa$N-Cu(II) and Cu(II)-$\kappa$N(HCA)$\kappa$O-Cu(II), which display disparate magnetic interactions.



Metal-ligand coordination is a well-established but still intriguing research area and has attracted much attention in the past decade, especially with the flourishing crystalline coordination polymers such as metal-organic frameworks. During the construction of coordination structures, it is commonly seen that small particles would grow bigger with time, for which Ostwald ripening is responsible [1]. Ostwald ripening is an equilibrium establishing process from a meta-stable phase to its thermodynamically stable phases, and is generally used as a post-synthesis process to modulate the morphologies of particles/crystals without changing the composition [2–4]. Thus, it should be intriguing to direct the equilibrium establishing process to develop new coordination structures.

Cyanuric acid (CA) and its ionic derivatives frequently serve as a linker in coordination chemistry due to its N- and O-sites for coordinate bonding and/or H-bonding. Many coordination complexes/polymers of CA to metal ions like Ca(II), Sr(II), Cu(II), Eu(II), Ba(II), and Ag(I) have been reported [5–14]. For Cu(II), the first reported coordination crystals with CA (**1**, structural formula $[Cu_1(H_2CA\text{-}\kappa N,N)_2(NH_3)_2]$ (-$\kappa$N,N indicates that the Cu atom coordinates two CA by the N-sites), synthesized by mixing cupric chloride and cyanuric acid in aqueous ammonia, is H-bonded coordination assembly formed from discrete coordination complexes (Fig. S1 in Supporting information) [13,14]. Nevertheless, the coordination polymeric structures of Cu(II)-CA have not been discovered yet. Our group have been interested in studying the competition of H-bonding and coordinate bonding and constructed a pair of interchangeable Ag(I)-melamine-CA coordination complex and coordination polymer [15–17]. Recently, we found that the growth of Cu(II)-CA coordination complexes (**1**) underwent a classic Ostwald ripening: small crystallites gradually formed large single crystals (Figs. 1A and B) within 3–5 days. The mass transfer from crystallites dissolving to big crystals growing inspired us to explore the possibility of controlling the mass transfer direction, *i.e.,* using the crystallites as resources to grow other coordination structures.

In this work, we reported on how to divert the equilibrium establishing process of meta-stable crystallites of **1** to cultivate Cu(II)-CA coordination polymers by adjusting the molar ratio of Cu(II) to CA (hereafter denoted as $M_{(Cu\text{-}CA)}$). We obtained two novel coordination polymers with different coordination sites of CA to Cu(II): from $\kappa$N–Cu–$\kappa$N to $\kappa$N–Cu–$\kappa$O, which displays disparate magnetic interaction in magnitude.

The seeds, Cu(II)-CA complex **1**, were synthesized by mixing $Cu(NO_3)_2$ and CA at a molar ratio $M_{(Cu\text{-}CA)} = 0.5$ in glass vials with aqueous ammonia (2 wt%). After shaking, the normal Ostwald

* Corresponding authors.
*E-mail addresses:* zheng.yanzhen@xjtu.edu.cn (Y.-Z. Zheng), Jingsan.Xu@qut.edu.au (J. Xu).
[1] These authors contributed equally to this work.

https://doi.org/10.1016/j.cclet.2023.108542
1001-8417/

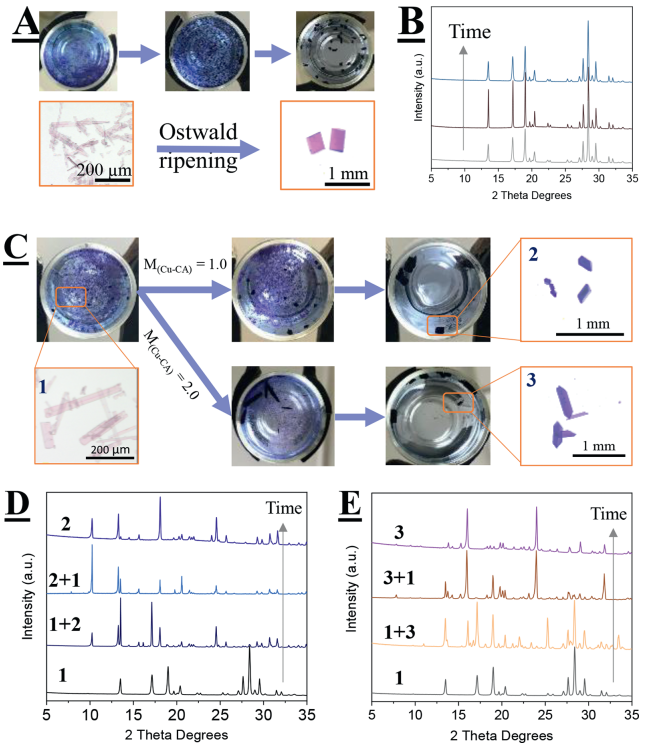


**Fig. 1.** (A) Photos illustrating Ostwald ripening of **1** from crystallites to large single crystals and (B) the corresponding powder X-ray diffraction (PXRD) patterns. (C) Photos of **1** transforming to **2** and **3**. PXRD patterns (D) from **1** to **2** and (E) from **1** to **3**.

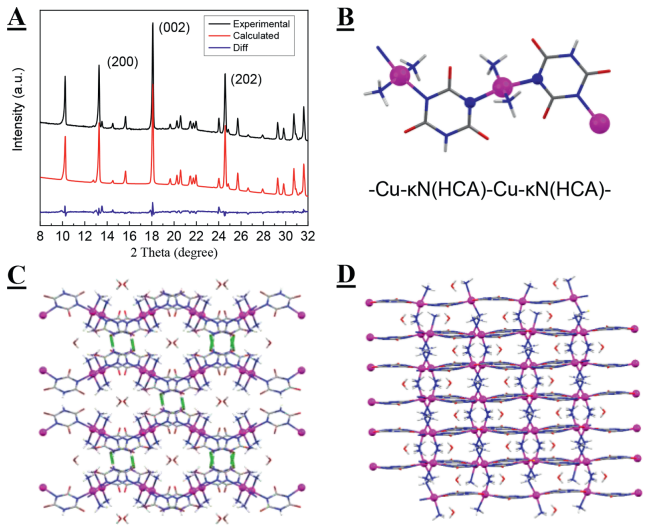


**Fig. 2.** Crystalline structure of **2**: (A) Calculated PXRD pattern; (B) Basic structural unit; (C) Extended view along [021]; (D) Extended view along [$\bar{1}$01]. Color codes: Cu, Magenta; O, red; N, blue; C, gray; H, white.

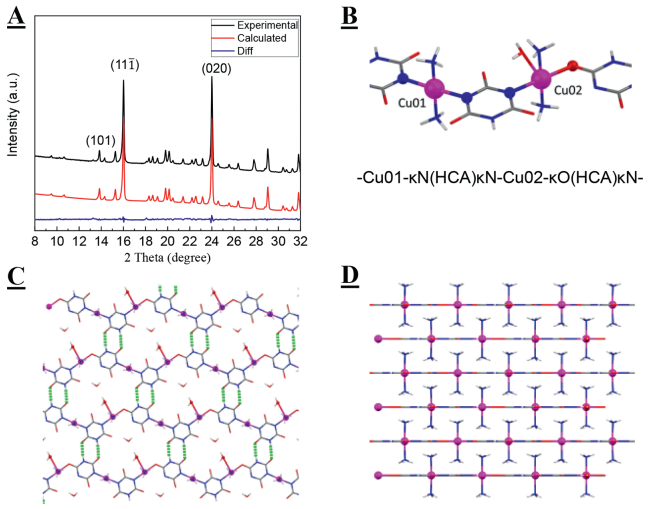


**Fig. 3.** Crystalline structure of **3**: (A) Calculated PXRD pattern; (B) Basic structural unit of **4**; (C) Extended view along [100]; (D) Extended view along [100]. Color codes: Cu, Magenta; O, red; N, blue; C, gray; H, white.

ripening would defer and the flakes of **1** were able to preserve for about three days. Then, different proportions of Cu(II) were added into the vials with the seed crystallites to adjust the total $M_{(Cu\text{-}CA)}$. After 2–3 weeks, the seeds gradually transformed into coordination polymers of Cu(II)-CA (Figs. 1C–E). Two coordination polymers were obtained, namely **2** and **3**, by adjusting the total $M_{(Cu\text{-}CA)}$ to 1.0 and 2.0, respectively. We screened more intervals of $M_{(Cu\text{-}CA)}$, but only found **2** and **3**. Moreover, higher ammonia concentration favored the generation of another copper cyanurate complex (**1***, Structural formula $[Cu_1(H_2CA\text{-}\kappa N,N)_2(NH_3)_2]\cdot[Cu_1(H_2CA\text{-}\kappa O,O)_2(NH_3)_4]$ (-$\kappa$O,O indicates that the Cu atom links two CA by the O-sites), whose PXRD and crystal structure were identical as previously reported (Fig. S2 in Supporting information) [14]. Nevertheless, the crystal transformation from coordination complexes to coordination polymers was still happenable under higher ammonia concentration (Table S1), although longer reaction time and more Cu(II) were needed. It is also found that adjusting the $M_{(Cu\text{-}CA)}$ at the commencement of the reaction did not change the crystal transformation. It should be noted that the big crystals of **1** after normal Ostwald ripening (Fig. 1A) upon the addition of extra Cu(II) were almost impossible to transform into **2** and **3** (no new crystals formed in months). Thus, the crystal transformation process from crystallites of **1** to **2** and **3** can be comprehended as a directed Ostwald ripening: The addition of extra Cu(II) favors the nucleation of Cu(II)-CA coordination chains in solution (which is more thermodynamically stable than crystallites of **1**) and the stable nuclei feeds on the discrete coordination complex to finally give rise to the coordination polymers.

The structure of **2** was refined in the monoclinic space group *C*2/*c* with the structural formula of $\{[Cu_2(HCA\text{-}\kappa N,N)_2(NH_3)_4]\cdot H_2O\}_n$ (Table S2 in Supporting information and Fig. 2A). The asymmetric unit comprises one Cu atom, one dideprotonated CA ($\mu_2$-CA), and two $NH_3$ (Fig. 2B). The four Cu–N dative bonds around the central Cu atom deform out of plane, constituting a flattened tetrahedral geometry. The structure shows **2** is a one-dimensional coordination polymer consisting of alternating $Cu(NH_3)_2$ and $\mu_2$-CA linked *via* Cu–$\kappa$N coordination bonds, forming a zig-zag chain structure of [Cu–($\mu_2$-CA)–Cu–($\mu_2$-CA)] ($NH_3$ are omitted for clarity). Neighboring chains are H-bonded *via* N–H···O between CA molecules, forming oval channels along *c* axis (Fig. 2C) which are filled by uncoordinated water molecules. The uncoordinated water molecules could be released upon heating as indicated by the gradual weight loss in thermogravimetric results (Fig. S3 in Supporting information). The CA molecules along one chain are non-coplanar, resulting in a rippled layer structure (Fig. 2D). The interlayer interactions are composed of $\pi$-$\pi$ interaction (3.895 Å) and H-bonds between $NH_3$ and CA.

Coordination polymer **3** crystalized in $P2_1/m$ space group, with an empirical formula of $\{[Cu(HCA\text{-}\kappa N,N)_1(NH_3)_2]Cu(HCA\text{-}\kappa N,O)(NH_3)_2(H_2O)]\cdot H_2O\}_n$, where -$\kappa$N,O indicates that the Cu atom links two CA by the N-site of one CA and the O-site of the other (Table S3 in Supporting information and Fig. 3A). The uncoordinated water molecules and coordinated water molecules in **3** could

be further confirmed by the two stages of weight loss upon heating before 275 °C (Fig. S3). The overall structure of **3** is like **2**, but with different coordinate modes around Cu atoms. In **3**, there are two Cu sites with different coordination numbers (Fig. 3B). One Cu is four-coordinate (Cu01) *via* two Cu–N($NH_3$) (2.002 Å) and two Cu–$\kappa$N (1.994 and 1.981 Å), forming a slightly twisted square plane. The other one, however, is five-coordinate (Cu02) *via* two Cu–N($NH_3$) (1.969 Å), one Cu–$\kappa$N (2.027 Å), one Cu–$\kappa$O (2.019 Å), and one Cu–O($H_2O$) (2.559 Å), making a distorted square pyramid. The alternating Cu01 and Cu02 develop the polymeric [Cu01–($\mu_2$–CA)–Cu02–($\mu_2$–CA)–Cu01–($\mu_2$–CA)] ($NH_3$ and $H_2O$ are omitted for clarity). The supramolecular structure is spread two-dimensionally *via* intermolecular H-bonds (average distance 2.018 Å) (Fig. 3C), forming sheets that are vertically stabilized by the H-bonds between $NH_3$ and $\mu_2$-CA. The $\mu_2$-CA and Cu atoms along the chain are situated on a perfect plane with a dihedral angle of 0°, remarkably different from **2** (Fig. 3D).

We found that the CA tautomerized from the *keto*-form in **1** to the *enol*-form in **2** and **3**. As shown in Table S4 (Supporting information), the average C=O bond length in **1** is shorter than that in **2** and **3**, indicating that the C=O bonds are weakened. Moreover, in FTIR spectra the peaks assigned to C=O (1732 $cm^{-1}$) weaken dramatically in the spectra of **2** and **3** (Fig. S4 in Supporting information), consistent with the elongated bond length of C=O, supporting the tautomerization of CA from *keto*-form to *enol*-form [15,17,18]. It is also observed that by gradually increasing the $M_{(Cu\text{-}CA)}$, the coordination modes in the final solids change from pure Cu–N (**1**, **2**) to mixed Cu–N and Cu–O (**3**), then to pure Cu–O (rouaite), which might be reasoned by that $Cu^{2+}$ is prone to attach with more electronegative sites. In mono-deprotonated CA (*keto*-CA), $Cu^{2+}$ is attracted by N-sites. In di-protonated CA, *keto*-CA tautomerizes to *enol*-CA and part of the electronegativity gradually shifts from the N-sites to the O-sites, so that the Cu–O can be energetically stable. Consistently, at extreme high $M_{(Cu\text{-}CA)}$, the solids are rouaite in which $Cu^{2+}$ is attached with the even more electronegative O-sites in $OH^-$, but not the CA or $NH_3$ molecules.

Near edge X-ray absorption fine structure (NEXAFS) spectroscopy at Cu $L_{3,2}$ edges was used to determine the oxidation state of the copper center. As shown in Fig. 4A, for **1** the $2p_{3/2} \rightarrow 3d$ and $2p_{1/2} \rightarrow 3d$ transition of Cu is located at 931.54 and 951.24 eV, respectively, indicating that the Cu ions were in the divalent state and there was no apparent charge transfer between ligands ($\mu_1$–CA) and cations [19]. For **2** and **3**, the $2p_{3/2} \rightarrow 3d$ transition of Cu(II) shifted to 931.04 and 931.14 eV, about 0.5 eV lower than **1**. The same trend was also found in $2p_{1/2} \rightarrow 3d$ transition. Although those values for **2** and **3** still fall in the regime of Cu(II), the slightly lower energy level of Cu(II) might hint at partial ligand-metal charge transfer ($\mu_2$–CA→Cu(II)), which is reasonable due to the larger electronegativity of $\mu_2$–CA than $\mu_1$–CA.

The dc magnetic susceptibility for **1** to **3** was measured at the temperature range of 2–300 K under an applied field of 1000 Oe (Figs. 4B–D), and the $\chi_M T$ products at room temperature are 0.376, 0.380 and 0.745 $cm^3$ K/mol, respectively, which correspond to the theoretical values for spin-only Cu(II) ion for **1** and **2** (0.375 $cm^3$ K/mol, $S = 1/2$) and two non-interacting Cu(II) ions for **3** (0.750 $cm^3$ K/mol, $S = 1$). Upon cooling, the $\chi_M T$ value of complex **1** shows a quite slow declining tendency until around 20 K, then quickly drops to the minimum value of 0.282 $cm^3$ K/mol at 2 K, which results from weak intermolecular antiferromagnetic (AFM) interactions and zero-field splitting effects [20–22]. The $\chi_M T$ products for **2** and **3** continuously decrease upon cooling, reaching almost zero at low temperatures, implying very strong intrachain AFM couplings mediated by the CA-bridges. The $1/\chi_M$ *vs. T* plots for **1** to **3** indicate that their magnetic susceptibility follows the Curie-Weiss law within a certain temperature range, and the best-fitting between 100 K and 300 K gives $C = 0.378$ $cm^3$ K/mol and $\theta = -0.308$ K for **1**; $C = 0.493$ $cm^3$ K/mol and $\theta = -85.768$ K for **2** and $C = 1.013$ $cm^3$ K/mol and $\theta = -107.642$ K for **3**. The negative Weiss constant $\theta$ supports the dominant AFM interactions in these compounds. The field-dependent magnetization data of three complexes were also measured at 2 K under the field of 0–5 T (Figs. S5–S7 in Supporting information). The magnetization for **1** rises smoothly with magnetic field and reaches 0.94 $\mu_B$ at 5 T without saturation, while for **2** and **3**, their magnetization exhibits very gradual increase and small magnitude, suggesting the existence of low residual paramagnetism and the occurrence of progressive decoupling of AFM couplings between Cu(II) ions through the external magnetic field [23].

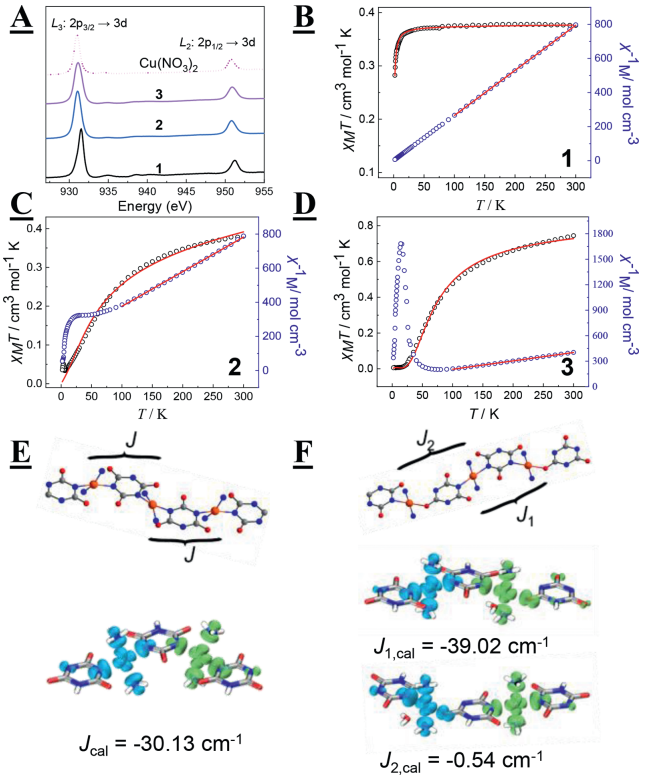


**Fig. 4.** (A) NEXAFS sepctra at the Cu $L_{3,2}$ edges. The temperature dependence of $\chi_M T$ and $\chi_M{}^{-1}$ for (B) **1**, (C) **2** and (D) **3**, respectively. The red solid lines are theoretical simulations based on the fitting procedure described in the text; The intrachain magnetic couplings and calculated spin density distributions of dimer fragments under broken symmetry (BS) states for (E) **2** and (F) **3**. (isovalue = 0.002 a.u., $\alpha$ spin in green and $\beta$ spin in blue). Color codes: Cu, orange red; O, red; N, blue; C, gray; H, white.

To investigate the existing magnetic couplings in three compounds, we adopted different means and models to acquire the specific exchange constants with respect to their crystal structures. The temperature dependence of $\chi_M T$ of **1** was fitted using PHI program [24] and the intermolecular magnetic interactions ($zJ'$) were treated with the mean-field approximation. The best-fitting of the magnetic data gives $zJ' = -0.46$ $cm^{-1}$ and TIP = $8 \times 10^{-5}$ $cm^3$/mol with $g = 2.0$, and this intermolecular exchange constant is in agreement with the Weiss constant $\theta$. While for **2** and **3**, their magnetic behaviors can be approximated as 1D uniform AFM chain with one isotropic interaction parameter $J$ and 1D alternating AFM chain with two interaction parameters $J_1$ and $J_2$ ($J_2 = \alpha J_1$) respectively, and the Hamiltonian can be expressed as $H = -J\sum S_i \cdot S_{i+1}$ and $H = -J\sum_{i=1}^{n/2}(S_{2i} \cdot S_{2i-1} + \alpha S_{2i} \cdot S_{2i+1})$ (Figs. 4E and F), where $\alpha$ is alternation parameter ($0 \leq \alpha \leq 1$), and $\alpha = 0$ and $\alpha = 1$ correspond to the cases of isolated pairs and a uniform chain. Therefore the experimental magnetic susceptibility data can be adequately de-

scribed by the Bonner-Fisher approximation for **2** (Eq. 1, $x = |J|/k_BT$) [25–28] and theoretical expressions derived by Hatfield for **3** ($0 \leq \alpha \leq 0.4$, Eqs. 2–8), $x = |J|/2k_BT$) [29–31], respectively. Considering the temperature-independent paramagnetism (TIP) and interchain interaction ($zJ'$), the temperature dependence of magnetic susceptibility for **2** and **3** can be best fitted by utilizing the parameters listed in Table S5 (Supporting information). The results demonstrated that intrachain CA-bridges were capable of transmitting strong AFM exchanges between Cu(II) ions, while the $\alpha$ value closer to zero in **3** indicates that the magnetic behavior of this 1D alternating chain approaches to a dinuclear Cu(II) system, and the different magnitude of $J_1$ and $J_2$ could be attributed to different bridging modes. Moreover, the differences of $\chi_M T$ products at low temperature range between **2** and **3** may originate from paramagnetic short chains after chain breaking in **2** and this part of magnetic susceptibility also follows the Curie law [27,28], which is reflected in the TIP terms that TIP = $1.86 \times 10^{-4}$ cm$^3$/mol for **2** is much higher than this value of $1.33 \times 10^{-5}$ cm$^3$/mol for **3**.

$$\chi_M = \frac{N\mu_B^2 g^2}{k_B T} \cdot \frac{0.25 + 0.074975x + 0.075235x^2}{1 + 0.9931x + 0.172135x^2 + 0.757825x^3} \quad (1)$$

$$\chi_M = \frac{2N\mu_B^2 g^2}{k_B T} \cdot \frac{A + Bx + Cx^2}{1 + Dx + Ex^2 + Fx^3} \quad (2)$$

$$A = 0.25 \quad (3)$$

$$B = -0.12587 + 0.22752\alpha \quad (4)$$

$$C = 0.019111 - 0.13307\alpha + 0.50967\alpha^2 - 1.3167\alpha^3 + 1.0081\alpha^4 \quad (5)$$

$$D = 0.10772 + 1.4192\alpha \quad (6)$$

$$E = -0.0028521 - 0.42346\alpha + 2.1953\alpha^2 - 0.82412\alpha^3 \quad (7)$$

$$F = 0.37754 - 0.067022\alpha + 6.9805\alpha^2 - 21.678\alpha^3 + 15.838\alpha^4 \quad (8)$$

Then calculations based on density functional theory combined with broken-symmetry (DFT-BS) approach were performed using Orca 4.2 program [32] to probe the main source of intrachain magnetic exchanges in **2** and **3** (see Supporting information for more details). The theoretical exchange coupling constants ($J_{cal}$) can be calculated through the energy gap between high spin (HS) and broken symmetry (BS) states as well as corresponding molecular spin expectation values (Eq. 9). Ultimately, the calculated coupling constants are $J_{cal} = -30.13$ cm$^{-1}$ for **2**, $J_{1,cal} = -39.02$ cm$^{-1}$ and $J_{2,cal} = -0.54$ cm$^{-1}$ for **3** which are very close to the experimental values. Moreover, the spin distributions from the calculations indicate only ~60% of the unpaired electrons are distributed on every Cu(II) site, while the rest of spin densities are mainly delocalized towards surrounding N and O atoms of the CA ligands, suggesting that magnetic exchanges are produced by the delocalization mechanism and involve the *d*-type magnetic orbitals of Cu(II) ions and sp$^2$ hybrid orbitals of ligand atoms. According to Kahn's model [33], the magnetic exchange constant possesses a direct proportion to the overlap density of both magnetic orbitals along the interaction pathway, and a larger degree of spin delocalization favors a stronger interaction. Checking the spin distributions of dimer fragments in **2** and **3**, we found that CA molecule as bridge ligand can transmit such interactions due to the large spin densities on it, while the smaller intrachain interaction in **3** ($J_2$) is caused by the extended magnetic exchange pathway and staggered arrangement of magnetic orbitals, which are derived from the coordination between Cu(II) ion and carbonyl oxygen.

$$J_{cal} = -\frac{E_{hs} - E_{bs}}{\langle S_{hs}^2 \rangle - \langle S_{bs}^2 \rangle} \quad (9)$$

In conclusion, we demonstrated that coordination complexes could be further transformed into coordination polymers upon proper incentives during crystal ripening. In our case, the copper cyanurate complex **1** were transformed into two different coordination polymers of copper cyanurate **2** and **3** by adjusting the molar ratio of Cu(II) to CA. Coordination polymer **2** and **3** displays similar structures but distinct coordination site connectivity. Intrachain CA-bridges in **2** and **3** can transmit strong AFM exchanges between Cu(II) ions. However, great disparity was observed in Cu(II)-$\kappa$N(HCA)$\kappa$N–Cu(II) and Cu(II)-$\kappa$N(HCA)$\kappa$O–Cu(II) pairs existed in **3** and the magnetic behavior of **3** is closer to a dinuclear Cu(II) system, demonstrating the importance of site connectivity in molecular magnetism. This work provides new insights for understanding crystal transformation in coordination chemistry.

## Declaration of competing interest

There are no conflicts to declare.

## Acknowledgments

The authors are grateful for the financial support from the Australian Research Council (No. DP190101607) and National Natural Science Foundation of China (No. 21971203). Central Analytical Research Facility (CARF) at QUT is greatly acknowledged for technical assistance.

## Supplementary materials

Supplementary material associated with this article can be found, in the online version, at doi:10.1016/j.cclet.2023.108542.

## References

[1] T. van Westen, R.D. Groot, Cryst. Growth Des. 18 (2018) 4952–4962.
[2] H. Xiao, C. Xue, P. Song, J. Li, Q. Wang, Appl. Surf. Sci. 337 (2015) 65–71.
[3] S. Kandula, K.R. Shrestha, G. Rajeshkhanna, N.H. Kim, J.H. Lee, ACS Appl. Mater. Interfaces 11 (2019) 11555–11567.
[4] C.C. Yec, H.C. Zeng, J. Mater. Chem. A 2 (2014) 4843–4851.
[5] M. Kalmutzki, M. Ströbele, F. Wackenhut, A.J. Meixner, H.J. Meyer, Angew. Chem. Int. Ed. 53 (2014) 14260–14263.
[6] M. Kalmutzki, M. Ströbele, F. Wackenhut, A.J. Meixner, H.J. Meyer, Inorg. Chem. 53 (2014) 12540–12545.
[7] M. Kalmutzki, X. Wang, A.J. Meixner, H.J. Meyer, Cryst. Res. Technol. 51 (2016) 460–465.
[8] J. Tang, F. Liang, X. Meng, et al., Cryst. Growth Des. 19 (2019) 568–572.
[9] F. Liang, L. Kang, X. Zhang, et al., Cryst. Growth Des. 17 (2017) 4015–4020.
[10] M.J. Kalmutzki, K. Dolabdjian, N. Wichtner, et al., Inorg. Chem. 56 (2017) 3357–3362.
[11] C.N.R. Rao, A. Ranganathan, V.R. Pedireddi, A.R. Raju, Chem. Commun. (2000) 39–40.
[12] C. Xiao, Y. Li, H. Lun, C. Cui, Y. Xu, J. Solid State Chem. 208 (2013) 127–133.
[13] P.G. Slade, M. Raupach, E.W. Radoslovich, Acta Crystallogr. Sect. B 29 (1973) 279–286.
[14] L.R. Falvello, I. Pascual, M. Tomás, E.P. Urriolabeitia, J. Am. Chem. Soc. 119 (1997) 11894–11902.
[15] P. Meng, A. Brock, X. Wang, et al., Inorg. Chem. 61 (2022) 2086–2092.
[16] P. Meng, Y. Xu, C. Yan, J. Xu, ACS Appl. Mater. Interfaces 12 (2020) 53125–53133.
[17] P. Meng, A. Brock, Y. Xu, et al., J. Am. Chem. Soc. 142 (2020) 479–486.
[18] T.J. Prior, J.A. Armstrong, D.M. Benoit, K.L. Marshall, CrystEngComm 15 (2013) 5838–5843.
[19] K.i. Shimizu, H. Maeshima, H. Yoshida, A. Satsuma, T. Hattori, Phys. Chem. Chem. Phys. 3 (2001) 862–866.
[20] O. Stetsiuk, A. El-Ghayoury, F. Lloret, M. Julve, N. Avarvari, Molecules 26 (2021) 2122.

[21] Q. Zou, J.C. Liu, X.D. Huang, S.S. Bao, L.M. Zheng, Chin. Chem. Lett. 32 (2021) 1519–1522.
[22] W. Chen, G. Zhou, Z. Gou, et al., Chin. Chem. Lett. 32 (2021) 838–841.
[23] P. Pandey, B. Kharediya, B. Elrez, et al., Dalton Trans. 46 (2017) 15908–15918.
[24] N.F. Chilton, R.P. Anderson, L.D. Turner, A. Soncini, K.S. Murray, J. Comput. Chem. 34 (2013) 1164–1175.
[25] J.C. Bonner, M.E. Fisher, Phys. Rev. 135 (1964) A640–A658.
[26] W.E. Estes, D.P. Gavel, W.E. Hatfield, D.J. Hodgson, Inorg. Chem. 17 (1978) 1415–1421.
[27] C. Kachi-Terajima, M. Ishii, T. Saito, et al., Inorg. Chem. 51 (2012) 7502–7507.
[28] M.M. Dîrtu, Y. Boland, D. Gillard, et al., Int. J. Mol. Sci. 14 (2013) 23597–23613.
[29] J.W. Hall, W.E. Marsh, R.R. Weller, W.E. Hatfield, Inorg. Chem. 20 (1981) 1033–1037.
[30] I. Castro, M.L. Calatayud, W.P. Barros, et al., Inorg. Chem. 53 (2014) 5759–5771.
[31] W. Huang, Y.H. Shui, X.X. Zhang, D.Y. Wu, Inorg. Chem. Commun. 33 (2013) 78–81.
[32] F. Neese, F. Wennmohs, U. Becker, C. Riplinger, J. Chem. Phys. 152 (2020) 224108.
[33] O. Kahn, Angew. Chem. Int. Ed. 24 (1985) 834–850.